Nanoscale Electro-Thermal Transport in Multi-Valence Cerium oxide Based Resistive Random Access Memory devices

M. K. Bera, M. Choudhary, R. Mittal, D. K. Tyagi, R. Sehrawat, A. K. Sharma

Abstract: Nanoscale heat transfer through conductive filaments made of oxygen vacancy in RRAM devices have been studied theoretically for multi-valence cerium oxide (CeO_2) based resistive switching material. A thermodynamic model is implemented for the movement of oxygen ions due to Julian heat during the set and reset conditions in CeO_2-RRAM device. A physics based numerical modeling is also developed on the basis of temperature and electric field enhanced relocation of oxygen vacancies inside CeO_2 to predict the accurate temperature build up inside conductive filaments.

Index Terms: RRAM, Rare-earth oxide, Nanoscale heat transports.

1 INTRODUCTION

The semiconductor industry continuously searching for emerging non-volatile memory (NVM) technology because of its escalating demands for highly scalable, low power consumption, cost effective, and fast speed memory solutions. In fact, the global emerging memory market is valued at US$ ~8 billion by 2022 with annual growth rate exceeding 45% during the forecast period of 2017 to 2022 [1]. Among many promising candidates, resistive random access memory (RRAM) is an emerging NVM technology which is based on switchable resistances by electrical stimulus [2-3]. In recent years RRAM draws sincere attention owing to its simple manufacturing process, low power consumption, ultra-fast programming speed, good scalability and compatible with complementary metal oxide semiconductor (CMOS) technology [4]. In order to obtain sustainable resistive switching characteristics, many competent physical mechanisms have been proposed. Among others, the idea of formation and breakage of oxygen vacancy assisted conductive filaments (CFs) has been widely recognized [2-3]. During the process of resistive switching, the shift from high-resistance state (HRS) to low-resistance state (LRS) is known as set process. In fact, LRS phenomena occurs owing to migration of non-lattice oxygen vacancies towards the electrode caused by the defect induced soft breakdown. Contrarily, the shift from the LRS to the HRS is known as reset process. Reset process is triggered by demolition of CFs by electric-field supported oxygen ion-hopping. However, when the electric current flows through the conductive filament, a substantial amount of Joule's heat is liberated, hence, creating a finite temperature distribution across the filament which in turn affects the SET/RESET transition. Besides, the stability of CFs is a major issue since it regulates the retention time of LRS.

- *M. K. Bera Department of Physics, Maharishi Markandeshwar (Deemed to be University), Mullana, Ambala (133207), Haryana, India. Email: m.k.bera@mmumullana.org*
- *M. Choudhary, R. Mittal, D. K. Tyagi, R. Sehrawat and A. K. Sharma, Department of Physics, Maharishi Markandeshwar (Deemed to be University), Mullana, Ambala (133207), Haryana, India.*

Meanwhile, for low power consumption, smaller reset current is always favorable but it often reduces the retention time because of the formation of CFs with smaller size [5]. Despite the fact that Joule heat is not a major contributor in reset process in case of bipolar switching, but it has significant influences in speeding up the dissolution of CFs. Nevertheless, the excessive formation of Joule's heat could destroy CFs when adequately high amount of current passes through CFs. Hence, thermal management inside CFs is the big issue and still needs to understand the underlying physical mechanisms in detail. Recently, rare-earth oxides (CeO_x, Gd_2O_3, Lu_2O_3, Dy_2O_3, Eu_2O_3, Yb_2O_3 etc.) based resistive switching memory devices have been demonstrated promising electrical performances [6-7]. Among others CeO_2 is very attractive because of its multi-valence characteristics. Therefore, in this work, a physics based numerical simulation is performed. It is based on the movement of oxygen vacancies present in CeO_2-based bipolar RRAMs by the applied external electric field as well as temperature generated inside CFs. This study provides a microscopic insight into the filament temperature formation and its possible way to dissipate the heat generated. Thermal management is the key to ensure reliable, repeatable and stable electrical performances of filamentary CeO_2-RRAM devices.

2 NUMERICAL MODELING AND SIMULATION OF CEO2-BASED RRAM DEVICES

2.1 Proposed device structure and switching material

Among many ReO_x, CeO_2 in particular has very interesting multi-valence property which is originated from its existence of two different valence states. Upon oxygen vacancy formation, CeO_2 can transform its oxidation state from full oxidation state i.e. Ce^{4+} (CeO_2) to sub-oxide state, Ce^{3+} (CeO_{2-x}). This happens upon exchange of two electrons from oxygen ion to Ce ion by the reduction of two Ce^{4+} ions into Ce^{3+} as per the following reaction [8]:

$$2\,CeO_2 + 2Al \rightarrow Al_2O_3 + {}^1/_2\,O_2 + V_0^{2+} \quad (1)$$

$$2CeO_2 \rightarrow Ce_2O_3 + {}^1/_2\,O_2 + V_0^{2+} \quad (2)$$

In this study, Al-doped CeO_x is considered. Because Al, being a strong electro-positive metal in the periodic table has been demonstrated its strong oxidization property [4]. Therefore, if an ultrathin Al layer is sandwiched between cerium oxide layers, it is expected that Al can remove oxygen ion from CeO_2 and become oxidized itself (AlO_x). This in turn will help to

produce more oxygen vacancies inside the CeO_x prior to vacancy formation process by applied electric field, thereby Al will help to form conductive filament more easily.

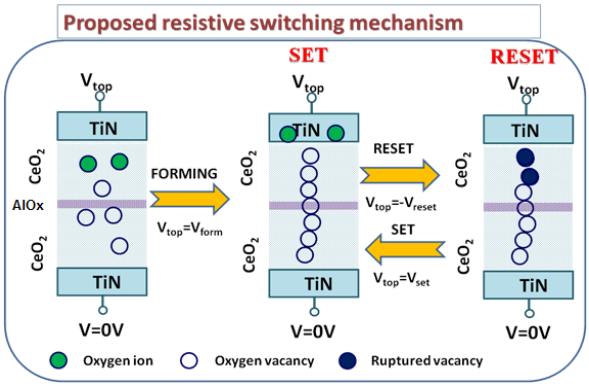

Fig. 1. *Resistive switching mechanism of CeO_2-based RRAM device.*

Besides, Al (work function ~4.28 eV) and TiN (work function ~5.69 eV) has large work function difference ~1.41 eV. As a result, Al may attract or repel charge carriers from or to bottom TiN electrode by the assistance of high local electric field required for charge transfer. The proposed resistive switching mechanism is schematically present in Fig. 1. RRAM devices usually have the dimension of ~100-200 nm having two metal electrodes sandwiched by an ultrathin (2-10 nm) insulator/oxide layer. The typical bias voltage and the electric field strength inside the insulator is usually ~ 1V and ~10^8 V/m, respectively [4]. Due to the presence of such a high electric field inside the insulator, a soft-breakdown occurs as a result of which a conductive path through the insulator will be created in the form of CFs. The formation of continuous CFs drive RRAM device into its low resistance state (set/on) while discontinuous CFs going back to high resistance state (reset/off). Once current passes through CFs, a significant amount of Joule heat is released generating a temperature distribution that effects the device operation and makes it unstable and unreliable. Therefore, a detail analysis of that temperature distribution is required so as to understand its underlying physical mechanisms and to facilitate necessary guidelines for effective RRAM device design. The numerical simulation is performed using SciLab/Matlab scripting.

2.2 Numerical modeling of Ceo_2-based RRAM devices

An auxiliary symmetric model is chosen with the cross section as shown in Fig 2 below. The dielectric layer corresponds to the metal oxide CeO_x. TiN metal electrode is chosen both as a bottom and top electrode. The constructed RRAM device parameters as well as various material parameter are listed in Table 1 and 2, respectively.

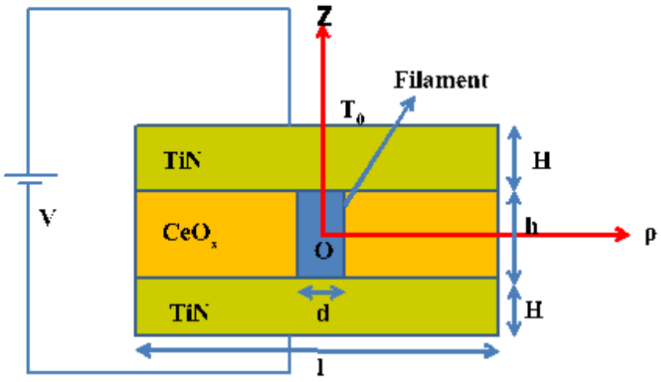

***Fig. 2**. Schematic of the proposed RRAM device structure. The top and bottom TiN electrodes are kept in ambient temperature while others are thermally insulated.*

Table 2 demonstrates the two different device dimensions those were considered for numerical modelling and simulation for this work. TiN top electrode was connected to a voltage source of 0.5 V while the bottom TiN electrode was grounded. The top and bottom TiN electrodes were kept with the surrounding temperature of 300 K. Proper electrical and thermal insulation of the side walls were considered during the simulation.

TABLE 1

Material parameters used in numerical modeling [9-11].

Material	*TiN*	*CeO_2*	*CeO_x*	*Ce*
Thermal conductivity, k (W/K.m)	*11.9*	*0.5*	*0.6*	*11.3*
Electrical conductivity, σ (S/m)	*10^6*	*10^{-2}*	*$2x10^4$*	*$2x10^6$*
Specific heat (J/kg.K)	*544.33*	*390*	*297*	*205*
Relative permittivity	*-∞*	*24*	*-∞*	*-∞*
Density (kg/m^3)	*5220*	*7600*	*7180*	*6760*

TABLE 2

Device dimension used in numerical modeling

Device /Dimension (nm)	*H*	*h*	*l*	*d*
Device I	*30*	*5*	*100*	*2*
Device II	*100*	*50*	*100*	*10*

2.3 Modeling of 1-D Electro-thermal transport in CeO_2-RRAM

Generally, thermal conductivity of any insulating layer is much less than that of CFs. Hence, one can consider filament transport will be essentially one-dimension (1-D). Now, let us suppose a conducting filament of height h is formed inside an insulator (CeO_2) layer sandwiched between two TiN electrodes under an external applied voltage V as shown in Fig. 2. The ends of the conducting filament are at the filament junction temperature, T_f, which will be influenced by the ambient temperature, T_a kept at the surface of TiN electrodes.

Now as per the steady state Joule's heat equation [4]:

$$-\nabla(k(T)\nabla T) = J.E \quad (3)$$

where E denotes electric field and J indicates current density inside the filament. As the value of δk/k is much less than the value of δT/T, one can assume thermal conductivity to be nearly constant. Further applying the Ohm's law (J= σE), the above equation can be reduced to the following form:

$$\nabla^2 T = -\frac{\sigma}{k} = -\frac{E^2}{k}.1/T \quad (4)$$

The solution of the above equation exhibits parabolic temperature distribution in the region of low heat where δT<<T is satisfied:

$$T(z) = T_f + E^2h^2/8LT_f[1-(2z/h)^2] \quad (5)$$

The maximum temperature can then be evaluated from the expression:

$$\delta T = E^2h^2/8LT_f \quad (6)$$

Meanwhile, during solving the above equation it was assumed that CFs junction temperature was the same as ambient temperature (i.e. $T_f=T_a$). However, this may not be true for nanoscale RRAM devices. But the CFs junction temperature can be significantly higher than the ambient temperature, hence, there is a need for correction. Since the thermal transport in TiN metal electrode is confined at nanoscale dimension, thus, TiN electrode will behave as a point contact heat source. On the other hand, the temperature dissemination at a distance of r can be approximated by analytical calculation by satisfying the condition that varying temperature will be same as ambient temperature while $r \rightarrow \infty$,

$$T(r) = (T_f-T_a)d/2r+T_a \quad (7)$$

Now, the amount of Joule's heat passes through a hemispherical surface of radius d/2 inside the TiN metal electrode can be expressed as: $2\pi (d/2)^2k_m\nabla T$. Where T calculated from equation (7) must be equal to that of delivered by the filament. The amount of heat supplied by CFs is now can be estimated as: $\pi(d/2)^2k_f\nabla T$ from equation (5). Henceforth, after doing some simple analytical calculation, the approximate expression can be derived as follows:

$$T_f = 1/2|T_a + (T_a^2 + \frac{\rho^2 V^2}{k_m k_f})^{0.5}| \quad (8)$$

Now, the corrected value of maximum temperature can be written as:

$$T_{max} = T_f + \delta T \quad (9)$$

By taking T_f value from equation (8) and δT from equation (6). For numerical estimation the following parameters were used: L ~4.88x10^{-8} WΩK^{-2}, T_a=300 K , and V= 0.5V. A substantial differences, δT= (T_{max}-T_f) between the junction and ambient temperature have been noticed. For instance, CeO_2-RRAM device I shows the temperature difference of ~1345 K while that for device II is ~1489 K. It can be noticed further that the junction temperatures calculated either by analytical or numerical methods are reasonably close as described in result and discussion section in detail. Yet, the maximum temperature predicted analytically is considerably higher. This inconsistency recommends that a trivial amount of heat flows radially outwards from CFs.

2.4 Radial temperature dissemination in CeO_2-RRAM

Although CeO_2 oxide possess very small thermal conductivity, however, heat flowing from CFs to TiN electrodes through the insulator can be important due to the presence of large area interfaces between CFs/CeO_2 and CeO_2/TiN electrode. Now, in order to understand the corresponding radial distribution of temperature, we have employed a simplified model of an ultrathin CeO_2 insulting layer where the transverse component of the temperature variation can be ignored. Hence, T can be further approximated to its average value: $\overline{T(\rho)}$.

So, the radial fluxes of the Julian heat flow can be written as:

$$\frac{1}{\rho}k_i h\left(\frac{\sigma}{2\rho}\right)\rho\left(\frac{\sigma}{2\rho}\right)\overline{T(\rho)} = 0 \quad (10)$$

where k_i thermal conductivity of CeO_2 insulator. Amount of heat absorbed by the TiN electrode is:

$$\frac{\kappa_m(T(\rho)-T_a)}{d} \quad (11)$$

Therefore, equating these two components of Julian heat flow one can easily obtained the following equation in the form of:

$$\frac{1}{\rho}\frac{d}{d\rho}\rho\frac{dT(\rho)}{d\rho} + \eta^2(T_a - \overline{T(\rho)}) = 0 \quad (12)$$

Where

$\eta = (2^{\kappa_m}/_{k_i Hh})^{0.5}$is the temperature reciprocal decay length. The solution of the above differential equation 12 can be found by employing Bessel function. The coefficient of the Bessel function can be easily calculated from the circumstances that the heat flux at ρ=d/2:

$\pi hd(\frac{dT(\rho)}{d\rho})$ is equal to the Joule's heat. After further simplification the solution of the above equation 12 can be written as:

$$\overline{T(\rho)} = T_a + V^2d\left|4hk_i\eta\left(\frac{\pi}{2}+\frac{2\pi}{\eta}\right)B_1\left(\frac{\eta a}{2}\right)\right| \quad B_0(\eta\rho) \quad (13)$$

where B_0 and B_1 are the modified Bessel function of zeroth and first kind.

Here in this study for numerical solution, we have used the abovementioned device parameters, which yields the temperature decay length of 1/η = 2.51 nm and 10.24 nm for device I and device II, respectively.

3 RESULTS AND DISCUSSION

Figure 3 and 4 demonstrates the temperature distribution along z-direction i.e. along oxide thickness direction for both types of devices.

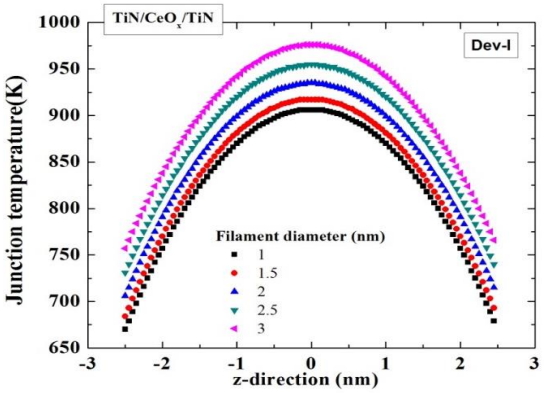

***Fig. 3**. Temperature distribution along z-direction (i.e. along oxide thickness) for the simulated TiN/CeO_x/TiN RRAM devices of type-I. The influence of conducting filament size is also investigated.*

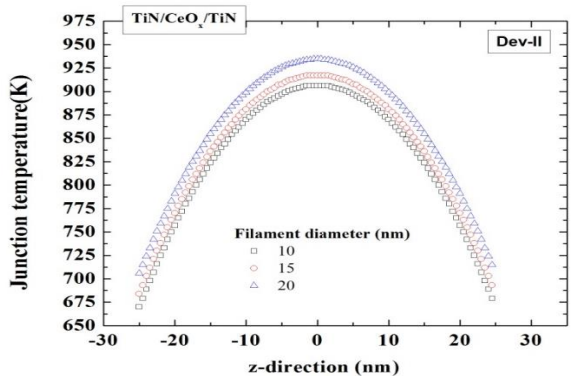

***Fig. 4**. Temperature distribution along z-direction of type-II device. The influence of conducting filament size is also investigted.*

It is evident that the temperature distributions are maximum at the center of the conducting filament. The heat is distributed in a hemispherical manner as predicted by the theoretical model. Besides, the influence of conducting filament size is also investigated.

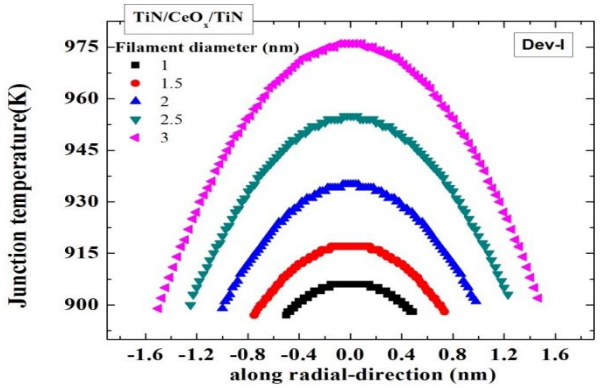

***Fig. 5**. Temperature circulation along radial direction (i.e. along conducting filament thickness) for the proposed type-I CeO_2 RRAM device.*

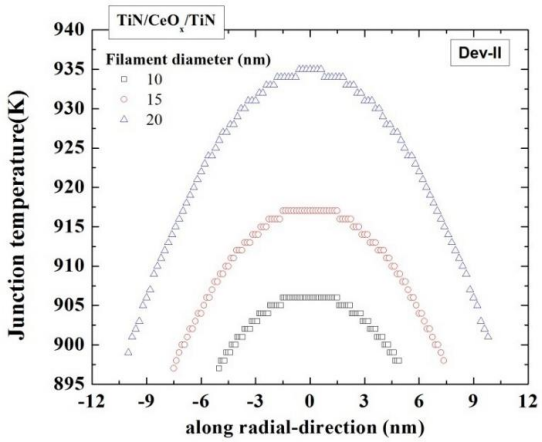

***Fig. 6**. Temperature dissemination along radial direction of the proposed type-II CeO_2 RRAM device. The influence of conducting filament size is also shown.*

It can be seen that as the filament size gets bigger the Joule heat becomes more prominent, consequently the peak temperature distribution shifts towards higher temperature as can be evidenced from both Figs. 3 and 4. Meanwhile, similar temperature distribution along the radial directions are shown in Fig. 5 and 6. It is worth noticed here that radial distribution of temperature is significant and increases drastically for increasing conducting filament diameter. Therefore, the correction for radial temperature distribution is necessary in order to accurately access the resistive switching behavior of CeO_2-based RRAM device design.

4 CONCLUSION

In this study, heat transport at nanoscale in oxygen vacancy related filamentary CeO_2-RRAM devices have been investigated. A common thermodynamic method has been utilized to assess the thermal effect on oxygen ion movements during set and reset operation in bipolar resistive switching devices. A physics based numerical model is developed in order to accurately predict the behavior of temperature generation inside the conductive filament for rare-earth oxide (CeO_2)-based bipolar RRAMs.

5 REFERENCES

[1] Orbis Research, “Global Next-Generation Memory Market Research Report- Forecast 2022,” 2017.
[2] H. Wang, X. Yan, “Overview of Resistive Random Access Memory (RRAM): Materials, Filament Mechanisms, Performance Optimization, and Prospects,” Phys. Status Solidi RRL, 1900073, 2019.
[3] Yen et al. “All Nonmetal Resistive Random Access Memory”, scientific reports, 2019.
[4] G. Roberto, C. Giovanni, In search of the next memory, Springer, 2017.
[5] R. Waser, R. Dittmann, G. Staikov, and K. Szot, “Redox-based resistive switching memories–nanoionic mechanisms, prospects, and challenges,” Advanced Materials, vol. 21, no. 25-26, pp. 2632-2663, 2009.
[6] Chen et al. “Bipolar Switching Properties of Neodymium Oxide RRAM Devices Using by a Low Temperature Improvement Method,” Materials, 10, 1415, 2017.
[7] Zhang et al. “High-k-rare-earth-oxide Eu2O3 films for transparent resistive random access memory (RRAM) devices,” J. Phys. D: Appl. Phys. 47 065302, 2014.
[8] Ismail et al. Effect of Bilayer CeO2−x/ZnO and ZnO/CeO2−x Heterostructures and Electroforming Polarity on Switching Properties of Non-volatile Memory Nanoscale Research Letters (2018).
[9] https://www.makeitfrom.com/material-properties/Ceria-Cerium-Oxide-CeO_2.
[10] C. L. Yaws, The Yaws Handbook of Physical Properties for Hydrocarbons and Chemicals, 2nd ed. Houston, TX, USA: Gulf, 2015.
[11] D. R. Lide, CRC Handbook of Chemistry and Physics, 88th ed. Boca Raton, FL, USA: Taylor & Francis, 2008.